# Minimizing Converter Requirements of Inductive Power Transfer Systems with Constant Voltage Load and Variable Coupling Conditions

Giuseppe Guidi, *Member IEEE,* Jon Are Suul, *Member IEEE*

*Abstract —*This paper proposes a combined design and control method for inductive power transfer systems that eliminates the need for over-rating the converters in applications where the coupling conditions vary significantly during operation. The method is developed for series-series-compensated systems with only one active power electronic converter and a diode rectifier connected directly to a constant voltage dc bus or a battery. The worst-case volt-ampere requirements are minimized by shaping the frequency characteristics of the system. Rated power flow during coupling variations is achieved by frequency control at constant voltage. Design guidelines are given to achieve close to unity power factor, constant current amplitude and minimum switching losses for the converter over the whole coupling range. Due to the simple system configuration requiring only one active converter with minimum rating, the method is deemed particularly suited for high-power applications. The properties of the investigated system configuration are demonstrated by theoretical analysis and time-domain simulations. Effectiveness and feasibility of the proposed method are also validated by experimental measurements from a small-scale laboratory prototype.

*Index Terms*—Frequency Control, Inductive Power Transfer, Magnetic Coupling, Power Control, Resonant Circuits

## I. INTRODUCTION

TECHNOLOGIES for wireless Inductive Power Transfer (IPT) have developed quickly during the last decades [1]-[4]. In particular, significant research and development efforts are currently directed towards battery charging of Electric Vehicles [2], [4]-[6]. Systems for static and dynamic wireless charging of road and rail vehicles have

been recently demonstrated with power levels reaching from a few kWs towards the MW-range [2], [4], [6]-[8].

High power IPT systems with loose coupling between the coils rely on capacitive compensation networks to ensure resonant operation and compensation of the large reactive power consumption resulting from low mutual inductance. The basic compensation networks – series-series (SS), series-parallel, (SP), parallel-series (PS) and parallel-parallel (PP) – are well established and have been object of extensive analysis and comparison [9]-[11]. However, optimization of design and control methods for improving efficiency and robustness to misalignment or variations in airgap distance, while fulfilling application specific requirements, is still an active research field with several approaches being pursued [10]-[18]. More complex compensation networks, including combinations of series-parallel connected capacitors [12], and/or additional inductors [19], [20] have also been proposed. Some of these topologies have shown promising performance in terms of reduced stress on power converters in case of variable load and/or variable coupling [12], [19]-[22]. However, the increased complexity and the requirement for additional reactive components make such topologies less preferable for very high power applications. Especially when reaching the MW power range, as for the applications in [8], [23], compensation networks with additional inductors and/or capacitors will imply significant added cost, complexity, weight and volume of the integrated system.

Amongst the simple IPT system topologies, SS compensation is often found most suited for high power battery charging applications [8] [11]. This is especially the case when load and coupling conditions may change during operation, since the SS topology results in small variations in resonant frequency [11]. SS compensated IPT systems can also be symmetrical, which leads to simpler coil designs, particularly when the input/output dc voltages are of similar magnitudes. Current-source behavior at the pickup-side is also desirable for battery quick-charging applications. Moreover, series compensation at sending-end allows for direct use of conventional voltage-source converter topologies, with no need for additional series inductance or other impedance conversion networks.

For any IPT system designed to operate with maximum efficiency at rated load in a given coupling condition, the efficiency can only drop when the coupling changes, unless active control is performed on the equivalent load resistance and/or on the resonant frequency of the system. At high power
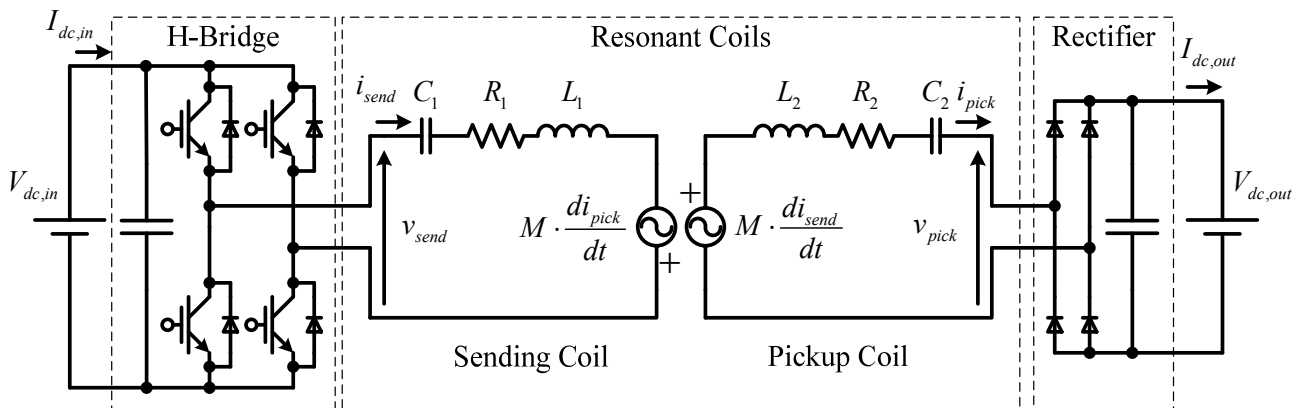
Fig. 1. Selected topology for IPT system with dc-source and CVL

levels, load matching while controlling the power flow to the desired level is normally achieved by using active power converters at both sides of the IPT link [4], [15]-[18]. However, using a diode rectifier at the pickup side rather than an active high-frequency high-power converter is a definite advantage in terms of system cost and complexity.

This paper addresses the general challenge of designing high power IPT systems suitable for operation with large variations in coupling between sending and pickup coils, due to relative movement or misalignment. Thus, the simple configuration of an SS-compensated system with a pickup-side diode rectifier interfaced to a constant dc voltage will be assumed. The sensitivity of the coupling against relative movement depends on the physical construction (i.e. shape, size, etc.) of the coils [11], [12]. However, this paper will not consider the electromagnetic design of the coils, but will instead analyze the fundamental properties of SS-compensated IPT systems transferring power between two fixed dc voltages. In particular, methods for shaping the frequency characteristics of such systems will be presented, and it will be discussed how these characteristics and the choice of control strategy will influence the rating requirements for the power electronic converters. On this basis, it will be demonstrated that a coordinated selection of resonant circuits and frequency control strategy can allow for minimum Volt-Ampere (*VA*) rating of the converters.

## II. BASIC CHARACTERISTICS AND LIMITATIONS OF SS-COMPENSATED IPT SYSTEMS OPERATED IN RESONANCE

In the simple SS-compensated system of Fig. 1, the sending coil is excited by the output voltage $v_{send}$ of an H-bridge converter. In general, $v_{send}(t)$ is a 3-level waveform with controllable fundamental frequency and amplitude, within the limit imposed by the input voltage $V_{dc,in}$. The ac signals at the pickup terminals of the resonant coils, $v_{pick}$ and $i_{pick}$, are rectified by a diode bridge whose dc terminals are connected to a Constant Voltage Load (CVL) $V_{dc,out}$.

In the literature, the characteristics of the system in Fig. 1 are usually studied by introducing two major assumptions, leading to the simple equivalent circuit in Fig. 2:

- Harmonic approximation; all the voltages and currents in the system are assumed to be sinusoidal.
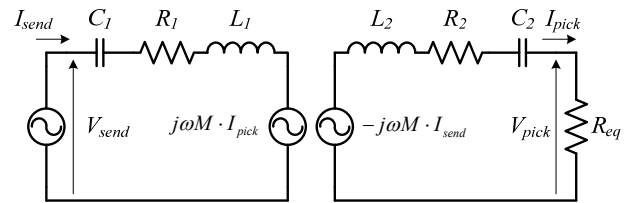- Load modelling with equivalent resistance.



Fig. 2. Equivalent circuit of SS-compensated IPT system using harmonic approximation and equivalent load resistance

Using phasors, the voltage limitations of the system introduced by the converters are therefore:

$$0 \leq V_{send} \leq \frac{2\sqrt{2}}{\pi} \cdot V_{dc,in}, \quad V_{pick} = \frac{2\sqrt{2}}{\pi} \cdot V_{dc,out} \quad (1)$$

The equivalent load is expressed as [24]:

$$R_{eq} = \frac{V_{pick}}{I_{pick}} = \frac{8}{\pi^2} \cdot \frac{V_{dc,out}}{I_{dc,out}} \quad (2)$$

It has been demonstrated in [4] that the maximum achievable power transfer efficiency of the system in Fig. 2 is given by:

$$\eta_{max} = \left( \frac{k \cdot Q}{1 + \sqrt{1 + (k \cdot Q)^2}} \right)^2 \quad (3)$$

The coupling coefficient $k$ and the quality factor $Q$ are expressed in terms of the coil self-inductances, $L_1$ and $L_2$, the mutual inductance $M$ and the series-equivalent resistances, $R_1$, and $R_2$, as:

$$k = \frac{M}{\sqrt{L_1 \cdot L_2}} \quad (4)$$

$$Q = \sqrt{Q_1 \cdot Q_2} = \sqrt{\frac{\omega_0 \cdot L_1}{R_1} \cdot \frac{\omega_0 \cdot L_2}{R_2}} \quad (5)$$

In order to maximize the power transfer capabilities and minimize the VA requirements of the sending-end converter, the resonant circuits at either side of the link are usually tuned to the same resonant frequency $\omega_0$:

$$\omega_0 = \omega_{0,send} = \frac{1}{\sqrt{L_1 C_1}} = \omega_{0,pick} = \frac{1}{\sqrt{L_2 C_2}} = 2\pi \cdot f_0 \quad (6)$$

The maximum efficiency in (3) is only achieved when the system is operated at resonance and the equivalent load at pickup is perfectly matched to the reflected impedance [11]:
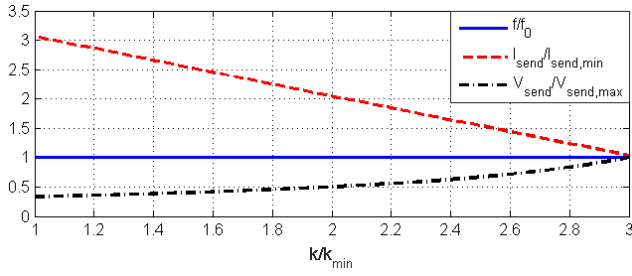
Fig. 3. Variation of sending voltage and current as function of coupling, assuming rated power flow and operation in resonance

$$R_{eq} = R_{eq,matched} = \frac{\omega_0 \cdot L_2}{Q_2} \cdot \sqrt{1+\left(k \cdot Q\right)^2} \qquad (7)$$

Assuming ideal lossless components, the steady-state power flow across the link, at the resonance frequency defined by (6), is calculated from Fig. 2 as:

$$P_0 = \frac{V_{send} \cdot V_{pick}}{\omega_0 \cdot M} \qquad (8)$$

When the magnetic coupling between sending and pickup coils changes, $M$ will change and power flow can be kept constant by regulating $V_{send}$. For rated power flow $P_{rated}$ at maximum and minimum coupling, the following holds:

$$P_{rated} = \frac{V_{send,max} \cdot V_{pick}}{\omega_{0,max} \cdot M_{max}} = \frac{V_{send,min} \cdot V_{pick}}{\omega_{0,min} \cdot M_{min}} \qquad (9)$$

The mutual inductances $M_{min}$, $M_{max}$ and the resonant frequencies $\omega_{0,min}$, $\omega_{0,max}$ are those corresponding to minimum and maximum coupling, respectively. Operation in resonance with controllable voltage amplitude implies that unity power factor will be maintained in the entire operating range of the mutual inductance. For a lossless system, this implies:

$$P_{rated} = V_{send,max} \cdot I_{send,min} = V_{send,min} \cdot I_{send,max} \qquad (10)$$

In this equation, $I_{send,min}$ is the current required to transfer the rated power at the maximum coupling (which corresponds to maximum voltage), while $I_{send,max}$ is the current required at the minimum coupling (which corresponds to minimum voltage). Using (9) and (10), the maximum $VA$ requirements of the H-bridge can be calculated as:

$$S_{send} = V_{send,max} \cdot I_{send,max} = \frac{\omega_{0,max} \cdot M_{max}}{\omega_{0,min} \cdot M_{min}} \cdot P_{rated} \qquad (11)$$

For most loosely coupled SS-compensated systems, it is reasonable to assume $L_1$ and $L_2$ as constants, resulting in constant $\omega_0$. As a result of (4), this implies that $M$ will be approximately proportional to the coupling coefficient $k$. Thus, (11) simplifies into [25], [23]:

$$S_{send} \approx \frac{k_{max}}{k_{min}} \cdot P_{rated} \qquad (12)$$

The equation above shows that the range of coupling conditions has major effect on the $VA$ requirement at sending-end when operating in resonance with voltage control. Indeed, the worst-case rating requirement for the sending end converter is approximately given by the ratio between the maximum and minimum coupling coefficients. Thus, the wider the variation of $k$, the higher the required $VA$ rating will be, regardless of the particular voltage and current levels. This
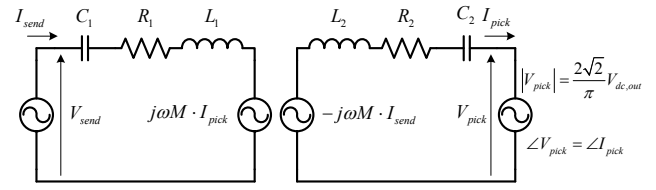


Fig. 4. Equivalent circuit of SS-compensated IPT system using harmonic approximation and CV load resulting from diode-bridge rectification

is illustrated in Fig. 3 for a case with a ratio of 3 between the maximum and minimum coupling. The figure clearly shows how the sending voltage and current will change with the coupling when conventional fixed-frequency operation in resonance is used and rated power flow is maintained. In the figure, $V_{send}$ and $I_{send}$ are normalized to their respective values at maximum coupling $V_{send,max}$ and $I_{send,min}$.

## III. IPT STEADY-STATE FREQUENCY CHARACTERISTICS WITH CONSTANT VOLTAGE LOAD

When studying the frequency characteristics of the original physical system in Fig. 1, the load cannot be modeled by an equivalent constant resistance (CR) as in Fig. 2. Instead, it must be taken into account that the amplitude of the load voltage $V_{pick}$ will remain constant while the load current $I_{pick}$ will change when the excitation frequency changes. Thus, the combined action of the diode rectifier and the constant dc voltage source result in the harmonic equivalent circuit of Fig. 4. It is noted that the dependent voltage source representing the load is influenced by the pickup current; in particular, the phase of the pickup voltage must be equal to the phase of the current that is driving the polarity switching of the diode bridge, resulting in non-linear behavior of the overall circuit.

Using conventional circuit theory and imposing the constraints described above, a closed form solution for the currents and voltages in the system can be found. The general solution including conduction losses results is a complicated equation that is not shown here due to space constraints. However, in the ideal case of loss-less coils, the power transferred to the load has a relatively simple expression:

$$P_{out} = \frac{V_{pick}^2 \cdot \sqrt{\omega^2\left(\frac{k^2}{x_u^2}-1\right)+2\omega_0^2-\frac{\omega_0^4}{\omega^2}}}{L_2\left(\omega^2\left(k^2-1\right)+2\omega_0^2-\frac{\omega_0^4}{\omega^2}\right)} = \frac{V_{pick}^2}{R_{eq}\left(\omega,x_u\right)} \qquad (13)$$

where the unbalance factor $x_u$ is defined according to:

$$x_u^2 = \frac{L_1}{L_2}\left(\frac{V_{pick}}{V_{send}}\right)^2 \qquad (14)$$

The expression in (13) is only valid when the resulting power flow is real and positive, marking the limits for continuous conduction mode operation of the diode rectifier. For $x_u \leq 1$, the frequency range where non-zero power transfer can take place is given by the roots of the second order equation in the denominator of (13):

$$\omega_L \leq \omega \leq \omega_U, \quad \omega_L = \omega_0 \cdot \sqrt{\frac{1}{1+k}}; \quad \omega_U = \omega_0 \cdot \sqrt{\frac{1}{1-k}} \qquad (15)$$

From (13) it can be seen that the power transfer at the

frequencies $\omega = \omega_L$ and $\omega = \omega_U$, will ideally approach infinity.

The situation is markedly different if $x_u > 1$; in that case the operating range is given by the solutions of the expression in the numerator of (13) and is restricted to $\omega'_L \leq \omega \leq \omega'_U$,

$$\omega'_L = \omega_0 \cdot \sqrt{\frac{1}{1 + k/x_u}}; \quad \omega'_U = \omega_0 \cdot \sqrt{\frac{1}{1 - k/x_u}} \quad (16),$$

while the power flow approaches zero at the boundaries.

Under the same assumption of loss-less coils, the argument of the impedance seen by the source in Fig. 4 is expressed as:

$$\angle Z_{send} = \angle \frac{V_{send}}{I_{send}} = \arctan\left( \frac{\left(1 - \frac{1}{x_u^2}\right) + \frac{\omega_0^2}{\omega^2}\left(\frac{1}{x_u^2} - 1\right)}{\sqrt{\left(\frac{k^2}{x_u^2} - 1\right) + 2\frac{\omega_0^2}{\omega^2} - \frac{\omega_0^4}{\omega^4}}} \right) \quad (17)$$

From (17), the key property of systems operated at $x_u = 1$ (referred to as balanced systems in this paper) follows:

$$\angle Z_{send}\big|_{x_u=1} = 0 \qquad \text{for all } \omega_L \leq \omega \leq \omega_U \quad (18)$$

Thus, a loss-less balanced system operated with CV load will maintain unity power factor at the sending end for all possible operating frequencies within the range in (15).

The system balanced according to the definition above is also a perfectly matched system in the sense of the classical definition derived from the concept of equivalent resistance. In fact, evaluating (13) for $x_u = 1$ and $\omega = \omega_0$ we get:

$$R_{eq}\big|_{\omega = \omega_0, x_u = 1} = \omega_0 \cdot k \cdot L_2 \quad (19)$$

Since (13) applies to loss-less coils with infinite $Q$, (19) coincides with the expression of the ideally matched load in (7). It has previously been shown that an optimally matched system is operated at the bifurcation limit [26]. For CR-loaded systems this means that for any load higher than the critical value in (19), the phase displacement between sending voltage and current will not be monotonous with frequency and will have two additional zero-crossings beside the one at the resonant frequency (6). A similar phenomena occurs for CV-loaded systems, as consequence of the sign-inversion of (17) around $\omega_0$ when $x_u$ crosses unity.

A direct comparison between the steady state characteristics of the IPT system described above with CR load equal to (19) and with CV load corresponding to $x_u = 1$ is shown in Fig. 5. The voltage at the sending end is kept constant in both cases. In the figure, the power has been normalized to the value at resonance defined by (8).

As expected, CR and CV characteristics coincide in case of lossless coils and resonant operation with $\omega = \omega_0$. However, significant differences emerge when considering off-resonant operation. In particular, the power flow is always bounded in case of CR load, even when loss-less coils are considered. Moreover, the constant power factor characteristic of balanced CV load is never observed in the CR case. Fig. 5 also shows that when losses are accounted for, CV-characteristics are strongly affected; however, the power flow still has two pronounced peaks close to the limit frequencies in (15). Furthermore, the equivalent sending-end impedance remains very close to resistive for all frequencies between the two
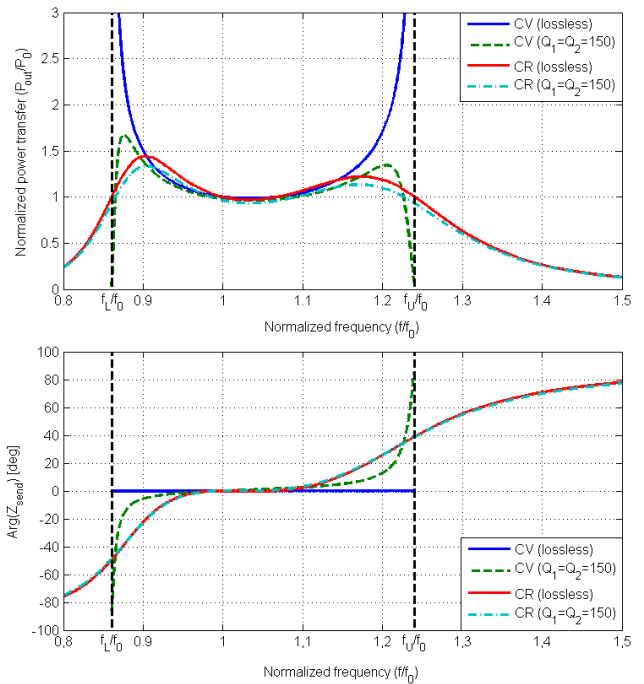


Fig. 5. Comparison between characteristics of SS- IPT system with optimally matched CR load at resonant frequency according to (19) and with CV load corresponding to $x_u = 1$, at $k = 0.35$

power peaks, implying close to unity power factor operation of the sending side converter for a relatively wide frequency range around the resonance frequency. Comparatively, CR characteristics are rather insensitive to losses, as long as the Q-factor remains within the range that can be expected for practical high power systems. Power peaks are much less pronounced for CR load and the variation of the sending-end power factor with frequency is much stronger.

It is emphasized that the characteristics shown in Fig. 5 are quite general, as they apply to all SS-compensated IPT systems that are designed to operate under perfectly matched load, regardless of the particular choice of voltage and current levels. The characteristics are drawn for $k = 0.35$; changing the coupling will affect the achievable CV operating range, as stated by (15). Higher coupling also leads to higher normalized power flow peaks, for the same Q-factors.

## IV. METHODS FOR ENHANCEMENT OF OUT-OF-RESONANCE POWER TRANSFER CAPABILITY

The characteristics of the ideal system, resulting from (13) and (18), suggest that by changing the operating frequency while keeping constant input voltage $V_{send}$, the power $P_{out}$ transferred to a CV load $V_{pick}$ with a certain coupling coefficient $k$ can ideally be regulated over the range:

$$P_0 \leq P_{out} \leq \infty; \qquad P_0(k) = \frac{V_{send} \cdot V_{pick}}{\omega_0(k) \cdot M(k)} \quad (20)$$

Moreover, the system will have unity power factor at both the sending and receiving sides over the whole regulation range. Fig. 5 shows that power control with constant sending end voltage and close to unity power factor can also be achieved for a system with reasonable losses in a wide

frequency range around the resonant frequency. This is in contrast with conventional super-resonant frequency control normally applied to series-resonant-load converters [27] or even with the more advanced dual voltage/frequency control [14], [28], [29]. Those methods achieve negligible turn-on losses of the switches, since they are always turned-on at zero current, but turn-off may take place at relatively high current. Associated losses are normally not negligible, especially when high-voltage IGBTs are used [30], [31].

The main problem of the constant-voltage, variable-frequency (CV-VF) control method is the relatively limited range achievable for the regulated output power. As indicated in Fig. 5, the range gets smaller as the quality factor of the coils decreases. Obviously, one should try to pursue the highest $Q$ possible for the design, in order to achieve highest possible efficiency (see (3)), but there are indeed practical limits dictated by component and material properties.

### A. Unbalancing the voltage transfer ratio for enhancing power transfer capability

The upper bound of the achievable power flow with frequency control can be increased by unbalancing the design so that the operation at rated voltage in resonance results in bifurcated characteristics. Using the unbalance factor $x_u$ defined in (14), a design rule for the coils is introduced as:

$$\frac{L_2}{L_1} = \left(\frac{G_{V,0}}{x_u}\right)^2 = \left(\frac{1}{x_u} \cdot \frac{V_{pick}}{V_{send}}\right)^2 ; \qquad 0 < x_u \leq 1 \qquad (21)$$

It is pointed out that in most conventional designs, unbalance in the opposite direction (i.e. $x_u > 1$) is deliberately added in order to avoid bifurcation and have monotonous characteristics for the argument of $Z_{send}$ [29], [32]. This is necessary when using control methods that rely on some kind of phase tracking for power flow control [14], [29].

In [33], the system is designed to operate beyond the bifurcation limit to extend the ZVS region in a way similar to what is proposed in this paper. However, no clear design rule is given, as the effect of unbalance is only indirectly evaluated by using the CR model.

The effect of unbalancing the design with $x_u < 1$ according to (21) is shown in Fig. 6 for the case with CV load. It is clear that a small amount of unbalance is very effective in increasing the power regulation range and also that it enhances the bifurcation in the phase characteristics of the system. In general, it should be expected that the unbalance will affect the maximum achievable transfer efficiency. However, as calculated in [11], the expected drop in maximum efficiency is not significant, as long as the unbalance is kept within 10-20%.

Even if the unbalancing is making the phase bifurcation more noticeable, the power factor at sending end remains very close to unity over the whole frequency range suitable for power regulation. However, the behavior at the AC terminals of the H-bridge may turn from inductive to capacitive (and vice-versa) with changes of the operating frequency and/or of the voltage ratio. Moreover, operation at the resonant frequency is guaranteed to be always at exactly unity power factor. This may be less than optimal for minimization of the
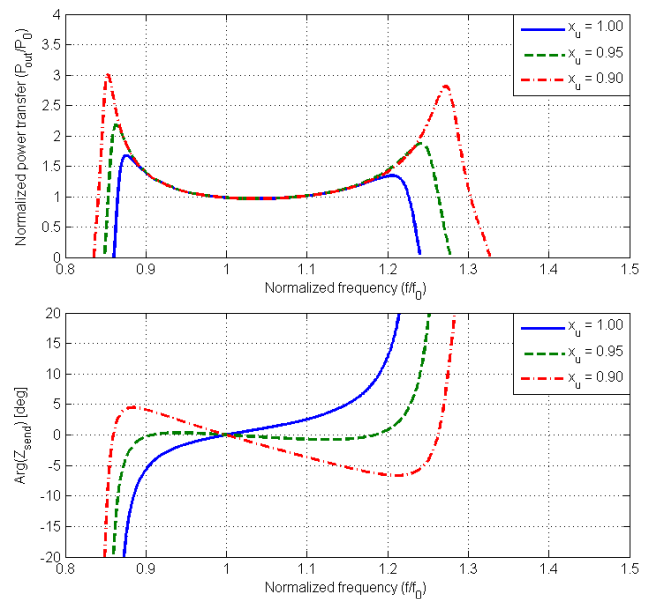


Fig. 6. Effect of design unbalance on IPT characteristics; Coils with $k = 0.35$, $Q_1 = Q_2 = 150$.

converter switching losses. As discussed in [34], [35], slightly inductive operation of the H-bridge is desirable, in order to achieve natural discharge of the output capacitance of the switches by the load current, resulting in zero-voltage switching (ZVS) with minimum loss.

### B. Detuning for ensuring ZVS conditions for the H-bridge.

It is possible to modify the phase characteristics of the IPT system by selecting different resonance frequencies at the sending and receiving sides [36]. A simple way of achieving slightly inductive impedance, consistently over the whole frequency range of interest for power regulation, is to deliberately introduce detuning of the compensation capacitances. Thus, the following generalization is proposed:

$$C_1 = x_c \cdot C_2 \cdot \frac{L_2}{L_1} \qquad (22)$$

When the capacitive detuning factor $x_c$ is unity, (22) reduces to the perfectly tuned condition defined by (6). The effect of detuning on the IPT frequency characteristics is shown in Fig. 7 and can be summarized as follows:

- $x_c > 1$ widens the range of power regulation in sub-resonant operation, $\omega_L < \omega < \omega_{0,pick}$. The impedance $Z_{send}$ seen by the H-bridge becomes slightly inductive over the whole frequency range of interest.
- $x_c < 1$ widens the range of power regulation in super-resonant operation, $\omega_{0,pick} < \omega < \omega_U$. The impedance $Z_{send}$ seen by the H-bridge becomes slightly capacitive over the whole frequency range of interest.

A small amount of capacitance detuning has negligible effect on the base power flow achievable in resonance and, as a consequence, on the expected efficiency. The design with $x_c > 1$ is particularly favorable, as it leads to ZVS with minimum turn-off current of all H-bridge switches during square-wave operation, resulting in very low switching losses over the whole frequency range.
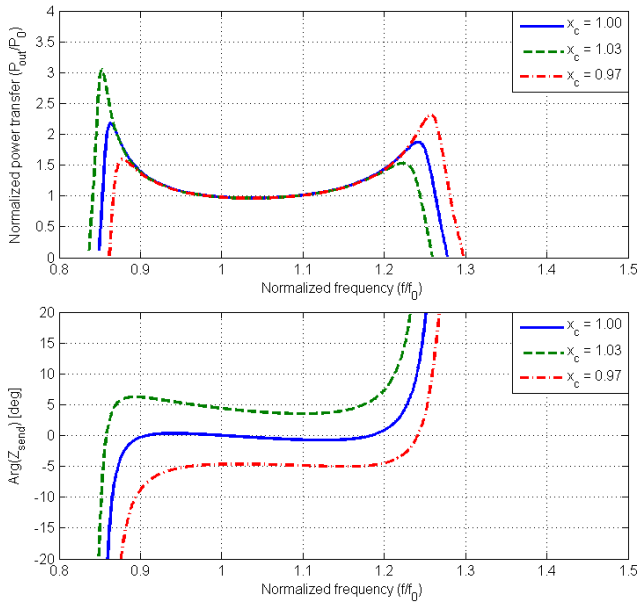
Fig. 7. Effect of capacitance detuning on IPT characteristics; Coils with $k$ = 0.35, $Q_1$ = $Q_2$ = 150 and unbalanced with $x_u$ = 0.95

## V.   POWER FLOW CONTROL WITH CONSTANT VOLT-AMPERE OPERATION FOR WIDE VARIATIONS OF COUPLING

The characteristics obtained in the previous section can be used as basis for controlling the power flow in case of wide variations of the coupling coefficient without incurring the worst-case component stress described in Section II.

A perfectly tuned, lossless, SS-compensated IPT system operated with square-wave modulation in resonance at nominal coupling $k = k_{nom}$ has rated power defined as:

$$P_{rated} = P_0\left(k_{nom}\right) = \frac{8}{\pi^2} \cdot \frac{V_{dc,in} \cdot V_{dc,out}}{\omega_0\left(k_{nom}\right) \cdot k_{nom} \cdot \sqrt{L_1 L_2}} \qquad (23)$$

As previously discussed, (23) is still a reasonable approximation if the Q-factor is sufficiently high, even if small unbalance and capacitive detuning are present. Assume that the coupling may change during operation in a range:

$$k_{nom} \le k \le k_{\max} \qquad (24)$$

Then, the frequency can be controlled over the sub-resonant range $\omega_L < \omega < \omega_0$ to keep rated power flow. Fig. 8 shows the static characteristics of the IPT in three different coupling conditions with indication of the resulting operating points at rated power under the proposed CV-VF control method. Rated power flow at close to unity power factor is always achieved, since the system is designed so that the peak power is higher than the rated value for maximum coupling:

$$\max_{\omega_L < \omega \le \omega_0} P_{out}\left(\omega, k_{\max}, x_u\right) > P_{rated} \qquad (25)$$

Since the sending voltage is constant, this implies almost constant sending current, in spite of the variation of the coupling in (24). For the particular case of Fig. 8, a variation of more than 300% on the coupling is possible without increasing the current rating of the H-bridge:

$$S_{send} = \max_{k_{nom} \le k \le k_{\max}} V_{send} \cdot \max_{k_{nom} \le k \le k_{\max}} I_{send} \approx P_{rated} \qquad (26)$$

This result should be compared with (12) that applies when conventional voltage controlled operation in resonance is
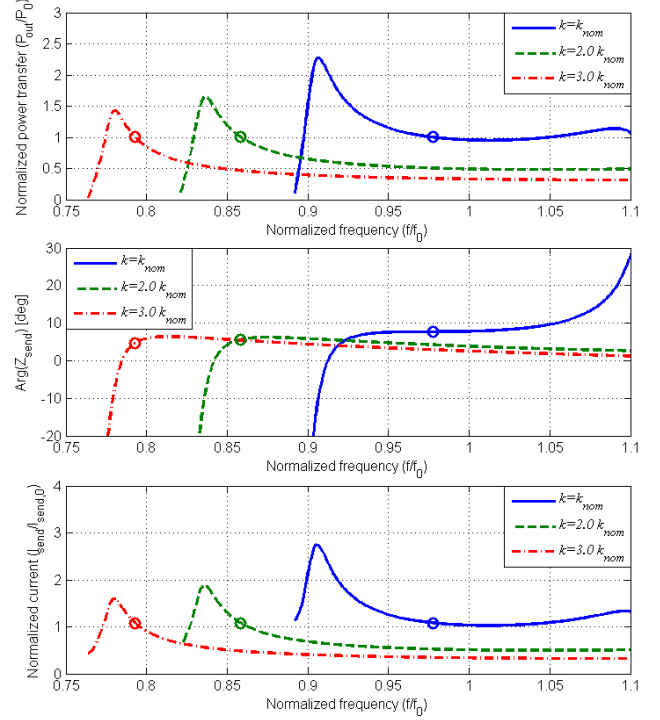


Fig. 8. IPT characteristics and operating points (marked with circles) at rated power, constant I/O voltage, variable coupling;
Coils with $k_{nom}$ = 0.2, $Q_1$ = $Q_2$ = 150;
Unbalance factor $x_u$ = 0.95; Detuning factor $x_c$ = 1.03
Frequency is normalized with respect to $f_0(k_{nom})$, and power is normalized to $P_0(k_{nom}) = P_{rated}$
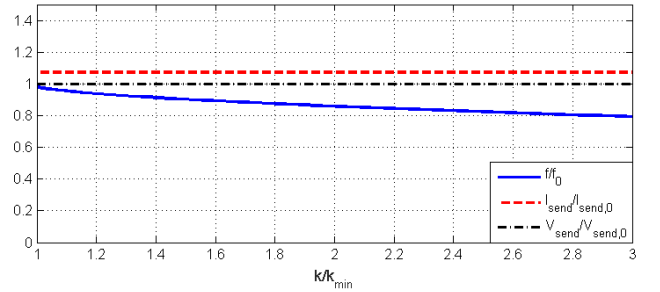


Fig. 9. Variation of sending voltage and current as function of coupling, assuming rated power flow and CV-VF operation

used. Fig. 9 shows how the coupling affects the sending current and voltage in case of rated power flow with the proposed CV-VF control strategy. In the figure, the voltage is normalized to its constant value $V_{send,0}$ and the current is normalized to the base value:

$$I_{send,0} = \frac{P_{rated}}{V_{send,0}} \qquad (27)$$

The results in Fig. 9 are in clear contrast with the behavior of the system operated in resonance as reported in Fig. 3.

The advantage of the proposed approach for design and control is made explicit by comparing results from time-domain simulations in Fig. 10. Operation of an IPT system designed for conventional voltage control at resonance (fixed frequency) is shown in Fig. 10 (a) and (b) when using the well-known phase-shift modulation method for the H-bridge
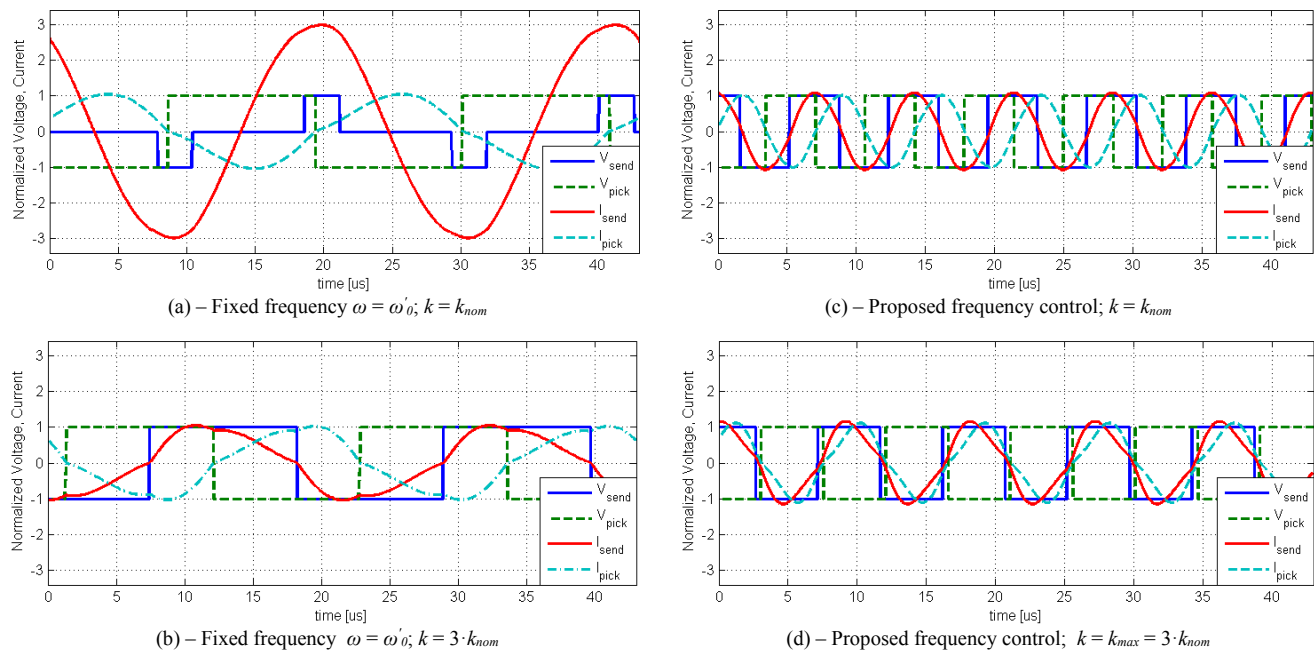
Fig. 10. Comparison between IPT voltages and currents at rated power and different coupling for two different design and control methods

[16]. Fig. 10 (c) and (d) show the IPT system designed with the characteristics of Fig. 8 and operated according to the proposed frequency control method. Steady state voltages and currents are shown for nominal and maximum allowed coupling, respectively.

The system operated at fixed frequency is designed with ideal balance and is perfectly tuned: $x_u = x_c = 1.0$. Its resonant frequency $\omega'_0$ is set by choosing the resonant capacitor values so that rated power flow $P_{rated}$ is achieved at rated voltage and maximum coupling. Assuming that the same coil design and I/O dc voltages are used for both systems, (23) results in:

$$\omega_0' = \frac{k_{nom}}{k_{max}} \cdot \omega_0 = \frac{\omega_0}{3.0} \qquad (28)$$

The results confirm that the worst-case current of the system operated in resonance and at fixed frequency is about three times higher than for the system designed and operated according to the proposed method, as predicted by (12). Fig. 10 (a) also shows that, because of the unity power factor operation at reduced voltage, the commutations of the H-bridge take place at very high current. In particular, considerable turn-on losses must be expected in the leading bridge leg. In contrast, the H-bridge in the proposed system design always operates in conditions corresponding to ZVS with low current, leading to very low switching losses.

It can be noted that it is indeed possible to use a double-stage conversion system for the system operated in resonance, with a dc-dc converter regulating the input dc voltage of the H-bridge for achieving the required variable ac voltage with square wave operation. However, such solution leads to increased complexity and cost due to the additional conversion stage. Moreover, the dc-dc converter is effective in reducing the switching losses but cannot solve the basic problem of increased sending current with variable coupling.

## VI. EXPERIMENTAL VERIFICATION ON A SMALL-SCALE IPT PROTOTYPE

To demonstrate the validity of the proposed approach, an experimental setup with parameters reported in TABLE I has been used. Two identical coils have been manufactured and mounted on a structure allowing for variable-distance operation, as shown in Fig. 11. A simple planar construction has been used for the coils, featuring an elongated spiral shape built over a rectangular ferrite back-plate serving as magnetic shield. As far as the proposed method is concerned, only the electrical parameters of the coils are relevant (self-inductance, coupling coefficient, quality factor); the particular shape and the magnetic construction of the coils has no influence and will therefore not be discussed in detail.

Measurements in Fig. 12 show the variation of the magnetic parameters of the coupled coils as function of the separation distance with perfect alignment. Over the considered range of distance, the coupling coefficient varies by a factor of 2.75, while the self-inductance remains almost constant.

The value of the resonant capacitors is designed so that rated power flow can take place in resonance at the nominal coupling. Moreover, 3% detuning ($x_c = 1.03$) is introduced in order to achieve slightly inductive power factor at the output of the H-bridge, resulting in close to optimal switching.

The quality factors of the prototype are estimated by considering the equivalent series resistance of all the components on the current path:

$$Q_{1,2} \approx \frac{\omega_0 \cdot L_{1,2}}{R_{1,2,coil} + \dfrac{\tan \delta}{\omega_0 \cdot C_{1,2}} + 2 \cdot R_{on,HB,D}} \qquad (29)$$

$$Q_1 = 172, \qquad Q_2 = 144, \qquad Q = \sqrt{Q_1 \cdot Q_2} = 157$$

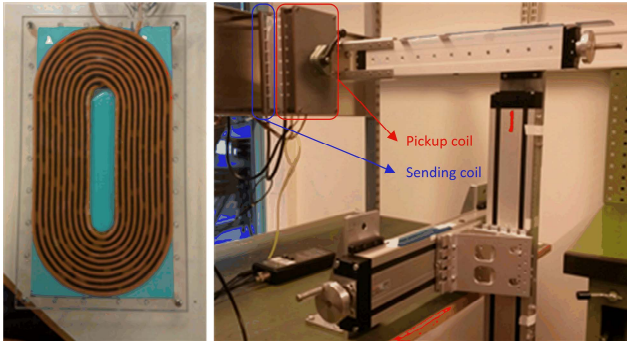Losses in the ferrite plates have been calculated using

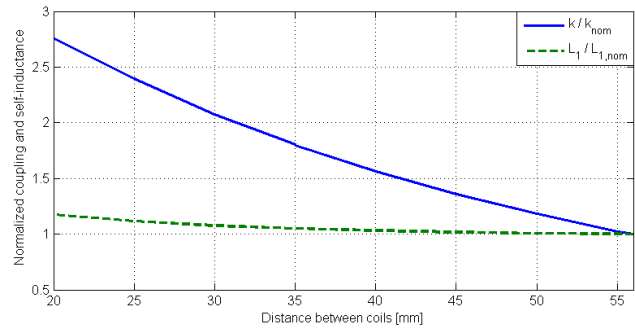Fig. 11 Coil winding and setup for variable-distance measurements.



Fig. 12. Variation of parameters of coupled coils with distance.



a) Simulation with ideal converters;
$Q = 157$, $k = k_{nom}$, $f = f_0 = 137 kHz$

b) Simulation with ideal converters;
$Q = 157$, $k = 1.56 \cdot k_{nom}$, $f = 123 kHz$

c) Simulation with ideal converters;
$Q = 157$, $k = 2.75 \cdot k_{nom}$, $f = 104 kHz$

d) Experimental results;
$k = k_{nom} = 0.205$, $f = f_0 = 137 kHz$

e) Experimental results;
$k = 1.56 \cdot k_{nom} = 0.320$, $f = 123 kHz$

f) Experimental results;
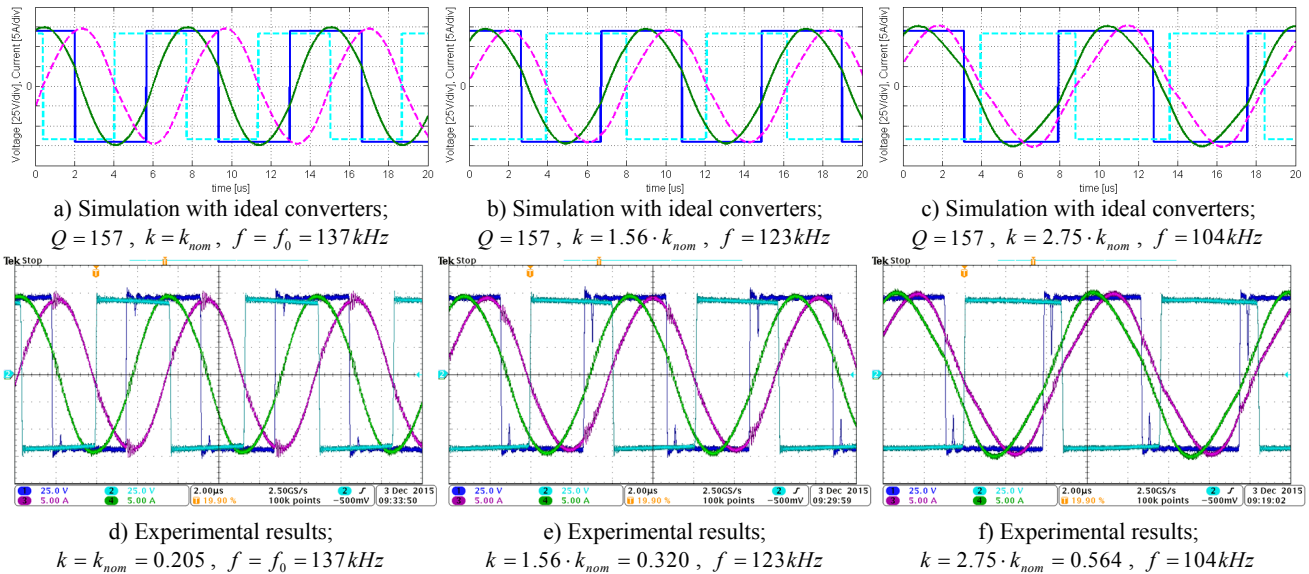$k = 2.75 \cdot k_{nom} = 0.564$, $f = 104 kHz$

Fig. 13 Comparison between simulations and experiments in different coupling conditions;
IPT system operated at rated I/O voltage and variable frequency, to achieve rated output power. The curves show:
Blue (solid): $V_{send}$ (25 V/div), Cyan (dashed): $V_{pick}$ (25 V/div), Green (solid): $I_{send}$ (5 A/div), Purple (dashed): $I_{pick}$ (5 A/div)

classical Steinmetz equation, since the currents are very close to sinusoidal. However, their contribution is small (less than 1W) and has therefore been neglected in (29).

As verified by evaluating (21) with the parameters of the setup, the system is designed with unbalance factor $x_u = 0.95$. According to Fig. 8, this is sufficient for the specified range of coupling while leaving margin for parameter uncertainties.

Experimental results taken from the prototype are shown in Fig. 13, together with the results of equivalent Matlab/Simulink simulations. In these simulations the H-bridge and the diode rectifier are assumed to be ideal, with zero on-resistance and infinitely fast commutations of switches and diodes. All the system losses are lumped into the equivalent series resistances at either sides of the IPT, whose values are calculated according to (29).

In the experiments, the DC-voltages at both sides of the link are kept at their nominal value by using a regulated DC power supply at the sending-end, and an electronic load operated in CV-mode at the pickup. For each measurement point, the coupling is set by changing the separation distance between the two coils. The system is started at the nominal resonant frequency $f_0 = 137$ kHz; the frequency is then slowly ramped down until the output power reaches the rated value.

TABLE I
PARAMETERS OF EXPERIMENTAL SETUP

| | |
|---|---|
| Nominal power, $P_0$ | 580 $W$ |
| I/O voltages, $V_{dc,in}$  $V_{dc,out}$ | 70.0 $V$, 66.5 $V$ |
| Coils | |
| Outer planar dimensions | 100 $mm$ by 200 $mm$ |
| Separation distance (min, max) | 20 $mm$, 56 $mm$ |
| Ferrite backplate (material, thickness) | 3C95, 4.1 $mm$ |
| Number of turns $N_1$, $N_2$ | 10, 10 |
| Litz wire (strand diameter, N. of strands) | 0.05 $mm$, 1575 |
| Self-inductance, $L_1$, $L_2$ (min, max) | 32.7 $\mu H$, 37.3 $\mu H$ |
| Coupling factor, $k$ (min, max) | 0.205, 0.564 |
| Measured resistance, $R_1$, $R_2$ (100$kHz$, 150$kHz$) | 45 $m\Omega$, 50 $m\Omega$ |
| Resonant capacitors | |
| Capacitance value, $C_1$, $C_2$ | 42.2 $nF$, 40.8 $nF$ |
| Dissipation factor, tan $\delta$ | 0.002 |
| H-Bridge | |
| Semiconductor devices | IRFP4768, 250V MOSFET |
| On-resistance, $R_{on,HB}$ (at $T_j = 100°C$) | 30 $m\Omega$ |
| Rectifier | |
| Semiconductor devices | IRFP4568, 150V MOSFET |
| On-resistance, $R_{on,D}$ (rev. cond., $V_{GS} = 0V$, $I = 10$ $A_{rms}$) | 45 $m\Omega$ |

As predicted by the characteristics in Fig. 8, the higher the coupling, the lower the resulting operating frequency. In this particular case, a variation of coupling between 0.205 and 0.564 (275% increase) leads to a frequency variation between 137 kHz and 104 kHz. As expected from the design, the power factor at the output terminals of the H-bridge remains constant, very close to unity and slightly inductive, in spite of the wide frequency range of operation. As a consequence, the amplitude of the currents does not change with coupling variations, resulting in close-to-constant efficiency at rated power over the whole coupling range. ZVS of the H-bridge takes place for all values of coupling.

For each operating point, Matlab/Simulink simulations are performed by using the same I/O DC voltages and the same operating frequency of the experiments. Resulting waveforms closely match the experimental results, validating the theory.

Measurements from the setup during the experiments in Fig. 13 result in about 0.920 dc-dc efficiency, regardless of coupling. This is due to the currents in the system being almost constant in spite of the large variation of coupling. Losses in the coils do increase with frequency, due to slightly higher ac resistance (see TABLE I), and so do the switching losses. On the other hand, ferrite losses are expected to decrease, due to lower flux density. In any case, the contribution of all frequency-dependent losses is minor in this case and could not be detected by measurements. According to (3), the maximum efficiency achievable by the setup at nominal coupling is calculated as 0.940. The 2% difference is mainly associated with the combined contribution of non-modeled loss components (switching losses in spite of ZVS, losses in the magnetic plates and in the metallic structures supporting the windings, losses in the dc-filtering capacitors etc.), measurement errors and uncertainty on loss parameters.

## VII.   Conclusion

A method for minimizing the rating requirements of power electronics converters in IPT systems intended to transfer rated power over a wide range of coupling conditions has been proposed and experimentally verified. It is shown that by properly designing the coils and compensation networks of a SS-compensated system with passive pickup, operation at rated power over a wide range of coupling can be achieved with constant currents. At the same time, close-to-ideal ZVS conditions for the sending side H-bridge converter can be maintained. The theory behind the proposed method is presented, based on analytical solution of the IPT circuit in case of CV-loading.

The wide operating range is achieved by designing the coils with a small unbalance, compared to the ideal and well-known condition of perfectly matched load, resulting in operation at rated load that is beyond the bifurcation limit of the system. At the same time, global ZVS conditions at rated power are ensured by slightly detuning the resonant frequencies of sending and pickup coils.

Matlab-based simulations and experiments on a small-scale prototype demonstrate the feasibility of the approach. Rated power flow with constant currents and constant I/O voltages

has been experimentally demonstrated for coupling variations as high as 275%. Simple, identical planar coils are used for the lab demonstrator and coupling is changed by varying the separation distance; however, the design principle can be applied to any coil design and coupling variation can be the result of arbitrary change of relative position and orientation.

Due to the simple structure of the converters and of the compensation networks, the proposed method is believed to be particularly suited for high power battery charging applications where the coupling may change widely during operation.

## References

[1]  G. A. Covic, J. T. Boys, "Inductive Power Transfer," *Proc. of the IEEE*, Vol. 101, No. 6, pp. 1276-1289, Jun. 2013

[2]  G. A. Covic, J. T. Boys, "Modern Trends in Inductive Power Transfer for Transport Applications," *IEEE Journal of Emerging and Selected Topics in Power Electronics*, Vol. 1, No. 1, pp. 28-41, Mar. 2013,

[3]  C. Fernández. O. García, R. Prieto, J. A. Cobos, J. Uceda, "Overview of different alternatives for the contact-less transmission of energy," in *Proc. of the 2002 28th Ann. Conf. of the IEEE Ind. Electron. Soc.*, IECON 2002, Sevilla, Spain, 5-8 Nov. 2002, pp. 13118-1323

[4]  S. Li, C. C. Mi, "Wireless Power Transfer for Electric Vehicle Applications," *IEEE Journal of Emerging and Selected Topics in Power Electronics*, Vol. 3, No. 1, pp. 4-17, Mar. 2015

[5]  G. Maggetto. P. Van den Bossche, "Inductive Automatic Charging: The Way to Safe, Efficient and User-Friendly Electric Vehicle Infrastructure, in *Proc. of the 18th International Electric Vehicle Symposium and Exhibition*, EVS-18, Berlin, Germany, 20-24 Oct. 2001, 12 pp.

[6]  A. Brecher, D. Arthur, "*Review and Evaluation of Wireless Power Transfer (WPT) for Electric Transit Applications*," U.S. Department of Transportation, Federal Transit Administration (FTA), FTA Report No. 0060, August 2014

[7]  S. Y. Choi, B. W. Gu, S. Y. Jeong, C. T. Rim, "Advances in Wireless Power Transfer Systems for Roadway-Powered Electric Vehicles," *IEEE Journal of Emerging and Selected Topics in Power Electronics*, Vol. 3, No. 1, pp. 18-36, Mar. 2015

[8]  J. H. Kim, B.-S. Lee, J.-H. Lee, S.-H. Lee, C.-B. Park. S.-M. Jung, S.-G. Lee, K.-P. Yi, J. Baek, "Development of 1-MW Inductive Power Transfer System for a High-Speed Train," *IEEE Trans. on Ind. Electron.*, Vol. 62, No. 10, pp. 6242-6250, Oct. 2015

[9]  C. S. Wang, O. H Stielau, G. A. Covic, "Design Considerations for Contactless Electric Vehicle Battery Charger," *IEEE Trans. on Ind. Electron.*, Vol. 52, No.5, pp. 1308-1313, Oct. 2005

[10]  C. Zheng, H. Ma, J.-S. Lai, L. Zhang, "Design Considerations to Reduce Gap Variation and Misalignment Effects for the Inductive Power Transfer System," *IEEE Trans. on Power Electron.*, Vol. 30, No. 11, pp. 6108-6119, Nov. 2015

[11]  R. Bosshard, J. W. Kolar, J. Mühlethaler, I. Stevanović, B. Wunsch, F. Canales, "Modeling and η-α-Pareto Optimization of Inductive Power Transfer Coils for Electric Vehicles," *IEEE Journal of Emerging and Selected Topics in Power Electronics*, Vol. 3, No. 1, pp. 50-64, Mar. 2015

[12]  J. L. Villa, J. Sallán, J. F. S. Osorio, A. Llombart, "High-Misalignment Tolerant Compensation Topology for ICPT Systems," *IEEE Trans. on Ind. Electron.*, Vol. 59, No. 2, pp. 945-951, Feb. 2012

[13]  M. Budhia, J.T: Boys, G.A. Covic, C. Huang, "Development of single-sided flux magnetic coupler for electric vehicle IPT charging systems," *IEEE Trans. on Ind. Electron.*, Vol. 60, No. 1, pp. 318-328, Jan. 2013

[14]  R. Bosshard, U. Badstubner, J. W. Kolar, I. Stevanovic, "Comparative evaluation of control methods for inductive power transfer," in *Proc. of the 1st Int. Conf. on Renewable Energy Research and Applications*, ICRERA 2012, Nagasaki, Japan, 11-14 Nov. 2012, 6 pp.

[15]  T. Diekhans, R. W. De Doncker, "A Dual-Side Controlled Inductive Power Transfer System Optimized for Large Coupling Factor Variations," in *Proc. of the 2014 IEEE Energy Conversion Congress and Exposition*, ECCE 2014, Pittsburgh, Pennsylvania, USA, 14-18 Sept. 2014, pp. 652-659

[16] T. Diekhans, R. W. De Doncker, " A Dual-Side Controlled Inductive Power Transfer System Optimized for Large Coupling Factor Variations and Partial Load," *IEEE Trans. on Power Electron.*, Vol. 30, No. 11, pp. 6320-6328, Nov. 2015

[17] H. H. Wu, A. Gilchrist, K. D. Sealy, D. Bronson, "A High Efficiency 5 kW Inductive Charger for EVs Using Dual Side Control, in *IEEE Trans. on Ind. Informatics*, Vol. 8, No. 3, pp. 585-595, Aug. 2012

[18] A. Berger, M. Agostinelli, S. Vesti, J. A. Oliver, J. A. Cobos, M. Huemer, "A Wireless Charging System Applying Phase-Shift and Amplitude Control to Maximize Efficiency and Extractable Power," *IEEE Trans. on Power Electron.*, Vol. 30, No. 11, pp. 6338-6348, Nov. 2015

[19] C.-S. Wang, G. A. Covic, O. H. Stielau, "Investigating an LCL Load Resonant Inverter for Inductive Power Transfer Applications," *IEEE Trans. on Power Electron.*, Vol. 19, No. 4, pp. 995-1002, Jul. 2004

[20] C.-Y. Huang, J. T. Boys, G. A. Covic, S. Ren, "LCL Pick-up Circulating Current Controller for Inductive Power Transfer Systems," in *Proc. of the 2010 2nd IEEE Energy Conversion Congress and Exposition*, ECCE 2010, Atlanta, Georgia, USA, 12-16 September 2010, pp. 640-646

[21] Y. Han, O. Leitermann, D. A. Jackson, R. M. Rivas, D. J. Perreault, "Resistance Compression Networks for Radio-Frequency Power Conversion," *IEEE Trans. on Power Electron.*, Vol. 22, No. 1, pp. 41-53, Jan. 2007

[22] M. Borage, S. Tiwari, S. Kotaiah, "Analysis and Design of an LCL-T Resonant Converter as a Constant-Current Power Supply," *IEEE Trans. on Ind. Electron.*, Vol. 52, No. 6, pp. 1547-1554, Dec. 2005

[23] G. Guidi, J. A. Suul, "Minimization of Converter Ratings for MW-scale Inductive Charger Operated under Widely Variable Coupling Conditions," in *Proc. of the IEEE PELS Workshop on Emerging Technologies: Wireless Power*, 2015 WoW, Daejeon, Korea, 5-6 June 2015, 7 pp.

[24] R. L. Steigerwald, "A Comparison of Half-Bridge Resonant Converter Topologies," *IEEE Trans. on Power Electron.*, Vol. 3, No. 2, pp. 174-182, Apr. 1988

[25] G. Guidi, "An apparatus and a method for wireless transmission of power between DC Voltage sources," Norwegian Patent application 20150087, January 2015

[26] C.-S. Wang, G. A. Covic, O. H. Stielau, "Power transfer capability and bifurcation phenomena of loosely coupled inductive power transfer systems," *IEEE Trans. on Ind. Electron.*, Vol.51, No.1, pp.148-157, Feb. 2004

[27] N. Mohan, T. M. Undeland, W. P. Robbins, "*Power Electronics: Converters, Applications, and Design*," 3rd Ed., John Wiley & Sons, 2003

[28] J. G. Hayes, N. Mohan, C. P. Henze, "Zero-Voltage Switching in a Constant Frequency Digitally Controlled Resonant DC-DC Power Converter," in *Proc. of the Third Ann. IEEE Applied Power Electron. Conf. and Expo.*, APEC'88, New Orleans, Louisiana, USA, 1-5 February 1988, pp. 360-367

[29] R. Bosshard, J. W. Kolar, B. Wunsch, "Control Method for Inductive Power Transfer with High Partial-Load Efficiency and Resonance Tracking," in *Proc. of the 2014 Int. Power Electron. Conf.*, IPEC-Hiroshima 2014 – ECCE Asia, Hiroshima, Japan, 18-21 May 2014, pp. 2167-2174

[30] M. Trivedi, K. Shenai, "Internal Dynamics of IGBT Under Zero-Voltage and Zero-Current Switching Conditions," *IEEE Trans. on Electron Devices*, Vol. 46, No. 6, pp. 1274-1282, Jun. 1999

[31] P. Randstad, H.-P. Nee, "On Dynamic Effects Influencing IGBT Losses in Soft-Switching Converters," *IEEE Trans. on Power Electron.*, Vol. 26, No. 1, pp. 260-271, Jan. 2011

[32] Y.-L. Lyu, F.-Y. Meng, G.-H. Yang, B.-J. Che, Q. Wu, L. Sun, D. Erni, J. L.-W. Li, "A Method of Using Nonidentical Resonant Coils for Frequency Splitting Elimination in Wireless Power Transfer," *IEEE Trans. on Power Electron.*, Vol. 30, No. 11, pp. 6097-6107, Nov. 2014

[33] C. Zheng, J.-S. Lai, R. Chen, W. E. Faraci, Z. U. Zahid, B. Gu, L. Zhang, G. Lisi, D. Anderson, "High-Efficiency Contactless Power Transfer System for Electric Vehicle Battery Charging Application," *IEEE Journal on Emerging and Selected Topics in Power Electronics*, Vol. 3, No. 1, pp. 65-74, Mar. 2015

[34] G. Ortiz, H. Uemura, D. Bortis, J. W. Kolar, O. Apeldorn, "Modeling of Soft-Switching Losses of IGBTs in High-Power High-Efficiency Dual-Active-Bridge DC/DC Converters," in *IEEE Trans. on Electron Devices*, Vol. 60, No. 2, pp. 587-597, Feb. 2013

[35] J. Huber, G. Ortiz, F. Krismer, N. Widmer, J. W. Kolar, "$\eta$-$\rho$ Pareto Optimization of Bidirectional Half-Cycle Discontinuous-Conduction-Mode Series-Resonant DC/DC Converter with Fixed Voltage Transfer Ratio," in *Proc. of the 28th Ann. IEEE Applied Power Electron. Conf. and Expo.*, APEC 2013, Long Beach, California, USA, 17-21 March 2013, pp. 1413-1420

[36] Z. U. Zahid, C. Zheng, R. Chen, W. E. Faraci, J.-S. Lai, M. Senesky, D. Anderson, "Design and Control of a Single-Stage Large Air-gapped Transformer Isolated Battery Charger for Wide-Range Output Voltage for EV Applications," in *Proc. of the 5th Annual IEEE Energy Conversion Congress and Exposition*, ECCE 2013, Denver, Colorado, USA, 15-19 September 2013, pp. 5481-5487

**Giuseppe Guidi** (M'00) received the Graduate degree from the University of L'Aquila, L'Aquila, Italy, in 1995, and the Ph.D. degree from the Norwegian University of Science and Technology (NTNU), Trondheim, Norway, in 2009.

He was involved in the field of power electronic drives from 1997 to 2004, joining first Fuji Electric R&D, Japan, as R&D Engineer and then SIEI SpA, Italy, as a Senior Engineer. In 2009, he joined Yokohama National University, Yokohama, Japan, as a Research Associate, working on power converters for electric vehicles. From 2011 he was a part-time Research Associate with NTNU, until joining SINTEF Energy Research, Trondheim, Norway, in 2013. His current research interests include power electronics, traction control, and drive systems for electric propulsion, as well as application of power electronics to renewable energy.

**Jon Are Suul** (M'11) received the M.Sc. and PhD degrees from the Department of Electric Power Engineering at the Norwegian University of Science and Technology (NTNU), Trondheim, Norway, in 2006 and 2012, respectively.

From 2006 to 2007, he was with SINTEF Energy Research, Trondheim, where he was working with simulation of power electronic converters and marine propulsion systems until starting his PhD studies. Since 2012, he has resumed a part-time position as a Research Scientist at SINTEF Energy Research while also working as a part-time post.doc researcher at the Department of Electric Power Engineering of NTNU. His research interests are mainly related to analysis and control of power electronic converters in power systems and for renewable energy applications.